A&A 591, A127 (2016)
DOI: 10.1051/0004-6361/201527183

Astronomy & Astrophysics

Shock-drift accelerated electrons and *n*-distribution

M. Vandas and M. Karlický

Astronomical Institute of the Czech Academy of Sciences, Fričova 258, 251 65 Ondřejov, Czech Republic
e-mail: vandas@asu.cas.cz

Received 13 August 2015 / Accepted 9 May 2016

ABSTRACT

Aims. By analyzing soft X-ray spectra observed during the impulsive phase of several solar flares, the *n*-distribution function of superthermal electrons has been detected. In the paper we try to answer the question of whether electrons with this type of distribution function can be produced in a shock, e.g. in a flare termination shock.
Methods. We use analytical and numerical methods to compute distribution functions of electrons accelerated by a shock.
Results. We analytically derive the distribution functions of reflected electrons at quasi-perpendicular shocks. We also consider the influence of the electrostatic cross-shock potential, shock curvature, and the role of the upstream seed population on these distributions. The computed distributions are compared with the *n*-distributions. We found that a high-energy part of the distribution of electrons reflected at a quasi-perpendicular shock can be very well fitted by the *n*-distribution in all the cases we studied. This provides a chance to detect the flare termination shock.

Key words. shock waves – acceleration of particles – Sun: flares

1. Introduction

Shock waves are natural elements of eruptive solar flares. In the standard CSHKP model (Carmichael 1964; Sturrock 1966; Hirayama 1974; Kopp & Pneuman 1976) of eruptive flares and in its three dimensional generalization (Aulanier et al. 2012), the shock waves are mainly generated at front boundaries of ejected plasma. Some of these shocks are observed as type II solar radio bursts (Dryer et al. 1998; Gopalswamy et al. 2013).

Besides these shocks, in the impulsive flare phase, the standard flare model predicts the shock located at the upper parts of the flare arcade, called the termination shock. Here, the plasma that outflows from the fast magnetic reconnection region (located above the flare arcade) is suddenly nearly stopped (Birn & Priest 2007). Generally, this shock can be quasi-parallel (near the top of the arcade, where the magnetic field is nearly perpendicular to the shock front) or quasi-perpendicular (at some distance from the arcade top, where the magnetic field is nearly parallel to the shock front).

The termination shock, as with any other shock, should accelerate electrons and thus produce a non-thermal distribution of electrons in its vicinity. This gives us a chance to detect it. On radio waves, the termination shock has been already detected (Aurass et al. 2002; Chen et al. 2015), and observations (Chen et al. 2015), as well as simulations (Guo & Giacalone 2012) indicate that it could be an efficient particle accelerator. However, these observations are very rare.

Therefore a question arises: if the termination shock can be also detected in some other types of emissions, e.g. in the line spectra in the soft X-ray range. To do this, the non-thermal distribution of electrons in the vicinity of the termination shock has to be determined. In this paper, assuming the shock-drift acceleration mechanism, effectively operating for quasi-perpendicular shocks (Leroy & Mangeney 1984; Wu 1984; Krauss-Varban & Wu 1989; Vandas 1989b; Vandas & Karlický 2011), we calculate this non-thermal distribution function. The cited theoretical works are supported by observational evidence of accelerated electrons in the vicinity of nearly perpendicular shocks, e.g. at the Earth's bow shock (Anderson et al. 1979), traveling interplanetary shocks (Potter 1981), which are often bow shocks ahead of coronal mass ejections (CMEs), and it is assumed that the shock drift mechanism contributes to the acceleration of electrons at the heliospheric termination shock (Fahr & Verscharen 2016).

Recently, Kulinová et al. (2011) analyzed the line spectra of three solar flares in the 3.40–6.05 Å X-ray range observed by RESIK instrument (Sylwester et al. 2005). Considering three silicon lines (5.22, 5.68, and 5.82 Å) that are only observed during the impulsive phases of these flares and using diagnostic methods for determination of the distribution function, they find that the ratios of these silicon lines can be explained only by an electron distribution function, which is much steeper than the Maxwellian one in the high-energy range (above 1 keV). As a prototype for these distributions, the *n*-distribution (Hares et al. 1979) is used arbitrarily (e.g. Seely et al. 1987). The *n*-distribution function is described in the next section. In the flares, studied by Kulinová et al. (2011), the parameter n of the *n*-distribution, which controls the steepness of the electron energy spectra, was estimated up to $n = 11$.

Meanwhile, some ideas that explain the physical origin of the *n*-distribution appear: (a) moving Maxwellian electron distribution in an electric current system or in a return-current of the beam plasma system (Dzifčáková & Karlický 2008; Karlický et al. 2012); or (b) the distribution of electrons accelerated in the strong double layer (Karlický 2012). Because these explanations still have some drawbacks, in this paper we search for further possibilities to explain the physical origin of the *n*-distribution detected in solar flares.

Therefore, in this paper, we study the distribution function of electrons accelerated in the shock and compare it with the *n*-distributions. We focus on the high-energy part of these

distributions because this has the main effect on intensities of these X-ray lines and their ratios. Moreover, it is expected that during the impulsive flare phase, when these X-ray lines were detected, the termination shock is generated. If some similarity between both these distributions is found then the n-distributions detected during impulsive flare phases could indicate that the n-distributions were formed in the shock wave and thus maybe in the termination shock.

2. The n-distribution function

The n-distribution function (Hares et al. 1979) is defined by

$$f_n(E) = \frac{n_\mathrm{e}}{E_n\,\Gamma\left(\frac{n}{2}+1\right)}\left(\frac{E}{E_n}\right)^{\frac{n}{2}} \mathrm{e}^{-\frac{E}{E_n}}, \tag{1}$$

where E is the particle kinetic energy, n_e is the number density, and Γ is the gamma function. The n-distribution function depends on two parameters, the number n and the characteristic energy E_n, which are related to the mean particle energy

$$\bar{E} = \left(\frac{n}{2}+1\right)E_n \tag{2}$$

and the most probable energy

$$E_p = \frac{n}{2}E_n. \tag{3}$$

For $n = 1$ the distribution is a Maxwellian distribution and its characteristic energy $E_n \equiv E_1 = k_\mathrm{B}T$, where k_B is the Boltzmann constant and T is the temperature. The n-distribution is expressed as a distribution per energy in Eq. (1), so

$$\int_0^\infty f_n(E)\,\mathrm{d}E = n_\mathrm{e}. \tag{4}$$

Keeping the mean particle energy $\bar{E}$ constant, the n-distribution for $n > 1$ has a steeper decrease in its high-energy part than the corresponding Maxwellian distribution ($n = 1$), and a higher n means a steeper decrease in general. When comparing observations with a model that uses the n-distribution, n and E_n are considered as free parameters.

The n-distribution function is used without a deeper physical justification, as a mathematical construct which, when used, fits observational data. However, physical processes that would generate n-distribution functions are searched. Some have been mentioned in the introduction and the other process is examined in the following sections. We find some resemblance here with the kappa distribution function (Vasyliunas 1968), which was arbitrarily used to describe distributions of solar wind electrons (Feldman et al. 1983) or magnetospheric particles (Krimigis et al. 1981), and only afterwards its physical meaning started to emerge (Livadiotis & McComas 2013). When compared to the Maxwellian distribution, the n- and kappa distributions represent two antipodes, the n-distribution function has a steeper (softer) energy tail than the Maxwellian distribution, while the kappa distribution has a harder energy tail. Both distributions are used to explain soft X-ray observations of solar flares, but in different cases (Kulinová et al. 2011; Battaglia et al. 2015).

3. Distribution functions of accelerated electrons

Leroy & Mangeney (1984) and Wu (1984) pointed out that nearly perpendicular collisionless shock waves are capable of accelerating electrons. These shocks act as a fast moving magnetic mirror, therefore Wu (1984) named the acceleration mechanism a fast Fermi process. Analysis of electron motion in the shock layer revealed that electrons were accelerated by the shock drift mechanism (Krauss-Varban & Wu 1989; Vandas 1989b); not only electrons reflected upstream are accelerated, but also electrons transmitted downstream.

Following Wu (1984), we assume that the shock is a plane shock wave and that the initial upstream electron distribution (seed particles) is Maxwellian,

$$f_\mathrm{i}(v) = \frac{n_s}{\pi^{\frac{3}{2}}v_s^3}\mathrm{e}^{-\frac{v^2}{v_s^2}}, \tag{5}$$

where n_s is the number density and v_s is the thermal velocity. The distribution function is normalized as

$$\int_0^\infty\int_0^\pi\int_0^{2\pi} f_\mathrm{i}(v)v^2\sin\alpha\,\mathrm{d}\varphi\,\mathrm{d}\alpha\,\mathrm{d}v = n_s, \tag{6}$$

where α is the pitch angle of electrons (the angle between the velocity vector of an electron and the ambient magnetic field vector) and φ is their (gyro)phase. Electrons interact with the shock wave and are either reflected upstream or transmitted downstream. During the (gyrotropic) process their velocity and pitch angle are modified. Their final velocity v and pitch angle α are uniquely determined (through their equations of motion) by the initial velocity v_i and pitch angle α_i, so we can symbolically write functional relationships $v(v_i, \alpha_i)$ and $\alpha(v_i, \alpha_i)$. Reversing these relationships, we get $v_i(v, \alpha)$, which specifies the initial velocity from the final values v and α. Using the Liouville theorem, the final distribution function after interaction, $\tilde{f}(v, \alpha)$, can be constructed:

$$\tilde{f}(v, \alpha) = f_i[v_i(v, \alpha)] \tag{7}$$

(we note that f_i is isotropic). The final distribution per energy is

$$f(E) = \frac{2\pi}{m_\mathrm{e}}\sqrt{\frac{2E}{m_\mathrm{e}}}\int_0^\pi \tilde{f}(v, \alpha)\sin\alpha\,\mathrm{d}\alpha, \tag{8}$$

with $v = \sqrt{2E/m_\mathrm{e}}$, where m_e is the electron mass. Equation (8) follows from Eq. (6) and an equation analogical to Eq. (4).

The expressions for $v_i(v, \alpha)$, in the case of reflected and transmitted particles, are known (e.g. Decker 1983; Vandas 1989a). They follow from simple kinematic considerations: electrons move adiabatically, i.e. they conserve their magnetic moment and the problem is treated in the de Hoffmann-Teller frame of the shock, where the induced electric field vanishes. The problem here is magnetostatic, electrons conserve their kinetic energy and they are reflected at or transmitted through the shock, which acts as a magnetic mirror with the loss cone angle θ_c, related to the shock jump by $\sin\theta_\mathrm{c} = \sqrt{B_1/B_2}$, where B_1 and B_2 are the upstream and downstream magnetic fields, respectively.

Utilizing the expressions for $v_i(v,\alpha)$, we obtain the distribution function of reflected electrons in the form

$$f_r(E) = \frac{2\pi}{m_e}\sqrt{\frac{2E}{m_e}}\int_{\mu_1}^{\mu_2} f_i(v_i)\,\mathrm{d}\mu \qquad E > E_B, \tag{9}$$
$$= 0 \qquad E \le E_B,$$

$$v_i = \sqrt{\frac{2E}{m_e}\left(1 + 4\mu\sqrt{\frac{E_B}{E}} + 4\frac{E_B}{E}\right)}, \tag{10}$$

$$\mu_1 = -\left(\sin^2\theta_c\sqrt{\frac{E_B}{E}} + \cos\theta_c\sqrt{1-\sin^2\theta_c\frac{E_B}{E}}\right), \tag{11}$$

$$\mu_2 = -\sqrt{\frac{E_B}{E}}, \tag{12}$$

where $\mu = \cos\alpha$, $E_B = \frac{1}{2}m_e V_B^2$, $V_B = V_{1n}/\cos\theta_{Bn}$, V_{1n} is the normal component of the upstream plasma bulk velocity with respect to the shock front, and θ_{Bn} is the angle between the shock normal and the upstream magnetic field. The quantity V_B represents the velocity of the magnetic mirror. It must be comparable to electron velocities for the electrons to be efficiently accelerated. These electrons have energies around 1 keV, so their velocity is very high in comparison to the plasma bulk velocity, therefore θ_{Bn} must be close to 90° (and we speak about a nearly perpendicular shock). The pitch angle $\alpha \in \langle 0, \pi\rangle$ is here defined in such a way, that electrons with $\alpha < \frac{\pi}{2}$ move towards the shock in the upstream region and away from it in the downstream region (i.e. $\mathbf{B}_1$ is oriented towards the shock; acceleration does not depend on the field orientation).

For electrons transmitted downstream we have

$$f_t(E) = \frac{2\pi}{m_e}\sqrt{\frac{2E}{m_e}}\int_{\mu_1}^{\mu_2} f_i(v_i)\,\mathrm{d}\mu, \tag{13}$$

$$v_i = \left\langle \frac{2E}{m_e}\left\{1 + 2\frac{E_B}{E} + 2\sqrt{\frac{E_B}{E}}\left[\mu - \sqrt{1-(1-\mu^2)\sin^2\theta_c + 2\mu\sqrt{\frac{E_B}{E}} + \frac{E_B}{E}}\right]\right\}\right\rangle^{\frac{1}{2}}, \tag{14}$$

$$\mu_1 = -\sqrt{\frac{E_B}{E}} \text{ for } E > E_B, \text{ otherwise } \mu_1 = -1, \tag{15}$$

$$\mu_2 = 1. \tag{16}$$

Equations (9)–(16) are valid for any isotropic initial distribution. When the Maxwellian distribution (5) is used, the integral (9) can be evaluated analytically; it reads

$$f_r(E) = \frac{n_s}{4\sqrt{\pi E_B E_s}}\left[\mathrm{e}^{\frac{4E_B}{E_s}\cos\theta_c\left(\sqrt{\frac{E}{E_B}-\sin^2\theta_c}-\cos\theta_c\right)} - 1\right] \times \mathrm{e}^{-\frac{E}{E_s}} \qquad E > E_B, \tag{17}$$
$$= 0 \qquad E \le E_B,$$

where $E_s = \frac{1}{2}m_e v_s^2$. The value of n_s in Eq. (17) refers to the number density of seed particles in Eq. (5). The number density

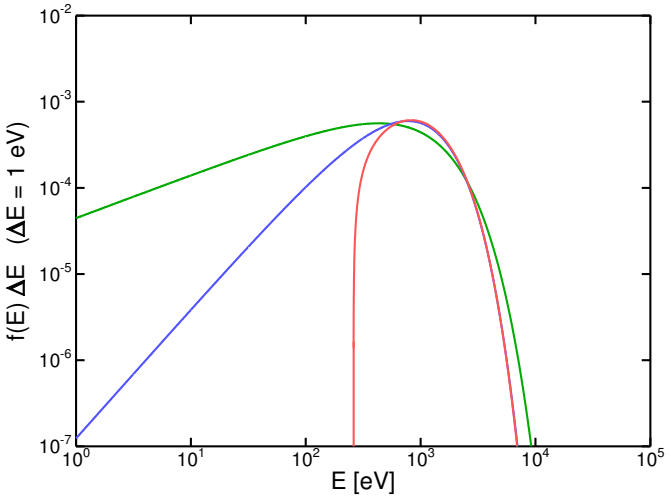

Fig. 1. Comparison of distribution functions: a Maxwellian distribution is indicated by the green line, an *n*-function with $n = 3$ by the blue line, and a distribution function of reflected electrons by the red line.

of reflected electrons is

$$n_r = \int_{E_B}^{\infty} f_r(E)\,\mathrm{d}E = \frac{n_s\cos\theta_c}{2}\left[1 + \mathrm{erf}\left(\sqrt{\frac{E_B}{E_s}}\cos\theta_c\right)\right]\mathrm{e}^{-\frac{E_B}{E_s}\sin^2\theta_c}, \tag{18}$$

where erf is the error function. Models usually need a distribution function normalized to its density. In the case of f_r from Eq. (17), its proper density is n_r, Eq. (18), not n_s; so n_s may be expressed via n_r from Eq. (18) and substituted into Eq. (17). The distribution function of transmitted electrons must be calculated numerically from Eq. (13).

4. Comparison of distribution functions of accelerated electrons with the *n*-distribution function

Figure 1 shows a comparison of three distribution functions. The Maxwellian distribution has $T = 10^7$ K (Eq. (1) with $n = 1$) and $n_e = 1$ (units of number density are not important for the present analysis, we use dimensionless quantities). The *n*-distribution function ($n = 3$) has the same mean particle energy as the Maxwellian distribution: $\bar{E} = \frac{3}{2}k_B T$, which determines $E_n \equiv E_3$ via Eq. (2). We see that the slope of the *n*-distribution function for higher energies is steeper than the Maxwellian slope. The profile of the distribution function of reflected electrons represents an ad hoc attempt to match the *n*-distribution function in its high-energy part. This was calculated from Eq. (17); parameters for the shock were taken from our papers on coronal shocks (Vandas & Karlický 2000, 2011): $V_{1n} = 1000$ km s^{-1} and $B_2/B_1 = 1.6$; the other parameters were $n_s = 3$, $E_s = k_B T/2$ and $\theta_{Bn} = 84°$. We see that, with these reasonable shock parameters, the high-energy part of the *n*-distribution function is met very well, also the positions of maximum coincide reasonably well. At lower energies, the distribution function of reflected electrons is cut at the energy E_B.

We also made similar calculations for transmitted electrons (not shown) which numerically evaluate the integral (13). The

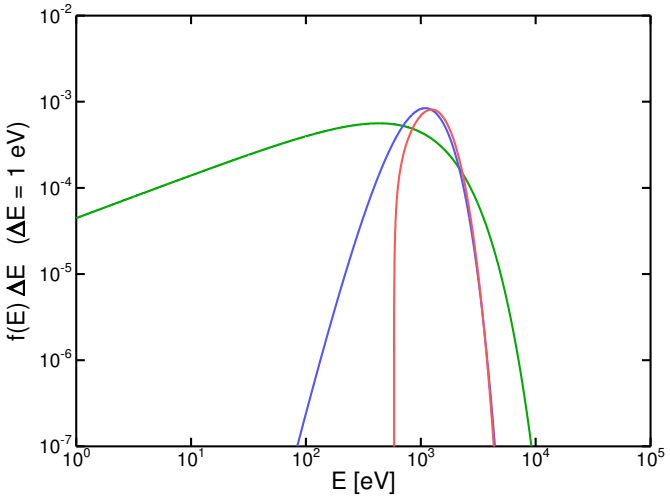

Fig. 2. Comparison of distribution functions: the Maxwellian distribution is indicated by the green line, an n-function with $n = 11$ by the blue line, and a distribution function of reflected electrons by the red line.

slope of their distribution in the high-energy part closely resembled the slope of the seed particles (i.e. Maxwellian one), so was not able to fit the n-distribution function. To be complete, there are also particles transmitted from downstream to upstream (Decker 1983), but their density is very low and their energy is only slightly modified, so that they even more closely resemble the seed particles (a Maxwellian distribution). Therefore we do not consider transmitted particles in further analysis and concentrate on reflected electrons.

Figure 2 is in the same format as Fig. 1 but it shows an extreme case of the n-distribution function, the function with $n = 11$. The Maxwellian distribution is the same as in Fig. 1. The $E_n \equiv E_{11}$ of the n-distribution function is determined by the same $\bar{E} = \frac{3}{2}k_\mathrm{B}T$. Reflected electrons have parameters $n_s = 30$, $E_s = k_\mathrm{B}T/7$, and $\theta_{Bn} = 86°$; the other parameters (notably of the shock) remained the same as for Fig. 1. The match of the higher-energy parts between the n-distribution function and the distribution of reflected electrons is quite good. We note that the extreme n-distribution, especially its high-energy part, also represents here the best fit in computations of the silicon line intensities and their ratios (Kulinová et al. 2011).

5. Influence of the electrostatic cross-shock potential and the shock curvature

To decelerate the upstream collisionless plasma, i.e. ions which bear an overwhelming part of the mass, an electrostatic field is formed in the shock layer which points upstream (e.g. Morse 1973). The electrostatic field does not disappear in the de Hoffmann-Teller frame and modifies the electron motion (Leroy & Mangeney 1984; Wu 1984); in kinematic considerations the conservation of the full energy (consisting of the kinetic and electrostatic potential energies) must be taken into account. The effect of the electrostatic potential is that it modifies the loss cone angle (e.g. Vandas 1989a) which is now denoted $\tilde{\theta}_\mathrm{c}$, into

$$\sin\tilde{\theta}_\mathrm{c} = \sin\theta_\mathrm{c}\sqrt{1+\frac{e\Delta\Phi}{E+2\mu\sqrt{EE_B}+E_B}}, \tag{19}$$

where $\Delta\Phi$ is the cross-shock potential and e is the elementary charge. We see that the loss cone angle is not constant but depends on the particle velocity and pitch angle. Eq. (11) is modified,

$$\mu_1 = -\left(\sin^2\theta_\mathrm{c}\sqrt{\frac{E_B}{E}} + \cos\theta_\mathrm{c}\sqrt{1-\sin^2\theta_\mathrm{c}\frac{E_B}{E}-\tan^2\theta_\mathrm{c}\frac{e\Delta\Phi}{E}}\right), \tag{20}$$

and instead of Eqs. (17) and (18) we have

$$f_r(E) = \frac{n_s}{4\sqrt{\pi E_B E_s}} \times\left[\mathrm{e}^{\frac{4E_B}{E_s}\cos\theta_\mathrm{c}\left(\sqrt{\frac{E}{E_B}-\sin^2\theta_\mathrm{c}-\frac{e\Delta\Phi}{E_B}\tan^2\theta_\mathrm{c}}-\cos\theta_\mathrm{c}\right)} -1\right]\mathrm{e}^{-\frac{E}{E_s}} \qquad E > E_m, \tag{21}$$

$$= 0 \qquad E \le E_m,$$

$$E_m = E_B + e\Delta\Phi\tan^2\theta_\mathrm{c} \tag{22}$$

$$n_r = \frac{n_s}{2}\left\{\sqrt{\frac{E_s}{4\pi E_B}} \times\left[\mathrm{e}^{\frac{4\cos\theta_\mathrm{c}\sqrt{E_B(E_m-E_B\sin^2\theta_\mathrm{c}-e\Delta\Phi\tan^2\theta_\mathrm{c})}}{E_s}} -\mathrm{e}^{-\frac{4E_B}{E_s}\cos^2\theta_\mathrm{c}}\right]\mathrm{e}^{-\frac{E_m+4E_B\cos^2\theta_\mathrm{c}}{E_s}} + \cos\theta_\mathrm{c}\mathrm{e}^{-\frac{E_B\sin^2\theta_\mathrm{c}+e\Delta\Phi\tan^2\theta_\mathrm{c}}{E_s}} \times\mathrm{erfc}\left(\sqrt{\frac{E_m-E_B\sin^2\theta_\mathrm{c}-e\Delta\Phi\tan^2\theta_\mathrm{c}}{E_s}} -2\cos\theta_\mathrm{c}\sqrt{\frac{E_B}{E_s}}\right)\right\}, \tag{23}$$

where erfc is the complementary function to the error function. For $\Delta\Phi = 0$, expressions (20), (21), and (23) reduce to expressions (11), (17), and (18), respectively.

According to Vaisberg et al. (1984), the potential jump is about 30–300 V at interplanetary shocks and 300–600 V for Earth's bow shock. However, in the de Hoffmann-Teller frame the electrostatic potential is highly suppressed owing to an out-of-plane magnetic field component inside the shock layer (Goodrich & Scudder 1984; Vandas 1991); instead of hundreds of volts, it is below a hundred.

Figure 3 demonstrates an influence of the electrostatic potential on reflected electrons. The profiles of the n- and Maxwellian distributions are taken from Fig. 1 and supplemented by the distribution of reflected electrons at a shock with the electrostatic potential. The value of 80 V was used for the total electrostatic potential. The parameters of the fit remained the same

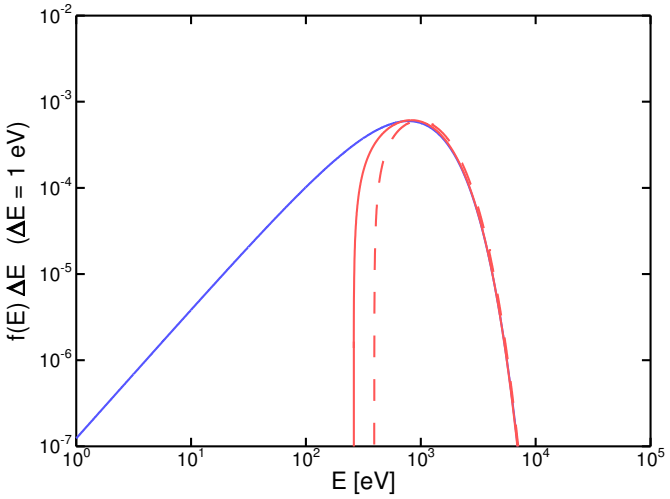

Fig. 3. Comparison of distribution functions: the n-function with $n = 3$ is indicated by the blue line (the same as in Fig. 1), the distribution function of reflected electrons ($\Delta\Phi = 0$) by the solid red line (the same as in Fig. 1), and the distribution function of reflected electrons when the cross-shock electrostatic potential is present ($\Delta\Phi = 80$ V) is indicated by the dashed red line.

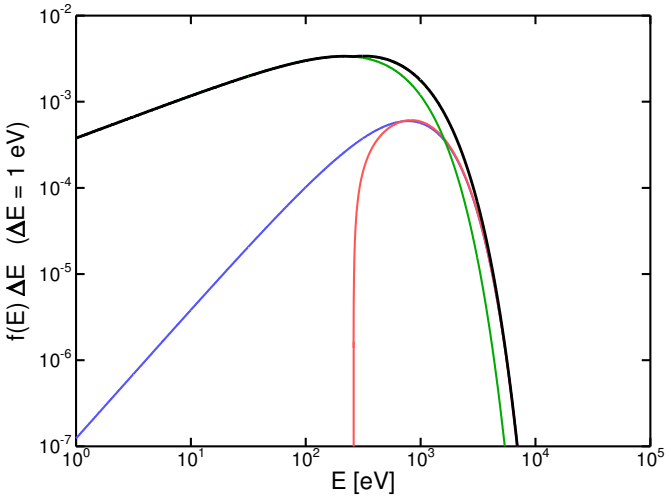

Fig. 4. Comparison of distribution functions: the n-function with $n = 3$ is indicated by the blue line, the distribution function of reflected electrons ($\Delta\Phi = 0$) by the red line, the seed (Maxwellian) distribution function for reflected electrons by the green line, and the total upstream distribution, i.e. the sum of the reflected electrons and the seed particles, by the black line. The blue and red lines are identical to the ones in Fig. 1.

as for Fig. 1, only n_s was increased to $n_s = 4$ in the case of $\Delta\Phi \neq 0$, because the electrostatic potential reduces the number of reflected electrons. We see that the cut-off energy increases, but the higher-energy part remains approximately the same, so the n-distribution is well fitted there.

Shocks in nature are curved. The role of the shock curvature has been investigated (Krauss-Varban & Burgess 1991; Vandas 1994). In this case, it is not possible to use the kinematic approach with the transformation into the de Hoffmann-Teller frame and it is necessary to calculate electron motions. However, Vandas (1994) has shown that the electron acceleration depends on the ratio of the shock thickness and the radius of curvature. When this ratio is small, electrons are accelerated as at a plane shock wave, i.e. their energy gain depends on the initial (≈final) θ_{Bn} where the particles start to interact with the shock. For coronal shocks, this ratio is extremely low (Vandas & Karlický 2000), so the results that are based on a plane shock wave (and presented above) are also applicable for curved shocks.

6. Role of the upstream seed population

Electrons are reflected upstream where their seed distribution propagates. So, in fact, the upstream distribution of electrons consists of the sum of these two distributions. This is shown in Fig. 4 which complements Fig. 1. The seed (initial) distribution fills the gap in the lower energy interval where reflected electrons are missing. However, the higher-energy slope is practically intact. Finally Fig. 5 complements Fig. 2 for $n = 11$. Qualitatively this is similar to the previous case, but the lower-energy part has very large values in comparison to the n-distribution.

The use of Maxwellian distributions as seed particles is crucial for the present analysis. For example, seed particles with a kappa distribution would not yield reflected electrons with an n-like distribution, but with a high-energy tail that is harder than a corresponding Maxwellian distribution.

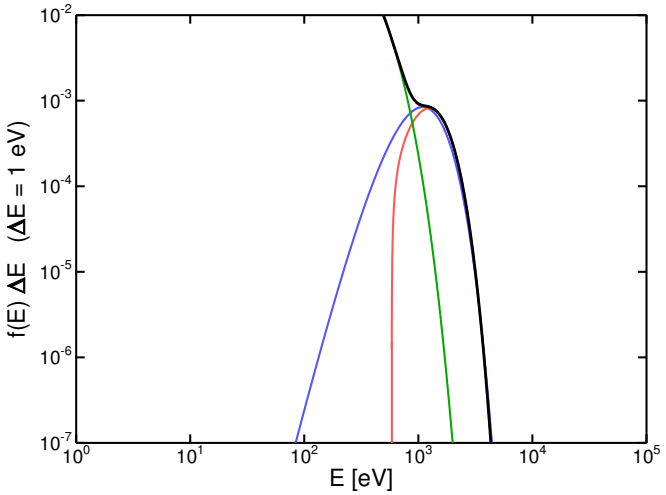

Fig. 5. Comparison of distribution functions: the n-function with $n = 11$ is shown by the blue line, the distribution function of reflected electrons ($\Delta\Phi = 0$) by the red line, the seed (Maxwellian) distribution function for reflected electrons by the green line, and the total upstream distribution, i.e. the sum of the reflected electrons and the seed particles, by the black line. The blue and red lines are identical to the ones in Fig. 2.

7. Conclusions

Using analytical methods, we derived the distribution functions of reflected electrons at quasi-perpendicular shocks. We compared the distribution functions of electrons reflected at shocks with and without the electrostatic cross-shock potential. We found that the low-energy cut-off increases, but the high-energy part of the distribution remains approximately the same. Owing to the relatively low level of the shock curvature, we can conclude that the computations in the plane-shock approximation are sufficient for this study.

In all treated cases, we found that a high-energy part of the distribution of electrons reflected at the quasi-perpendicular shock can be very well fitted by the n-distribution. Therefore the n-distributions detected in the impulsive flare phase of some

solar flares could be formed by the shock wave. Moreover, because during the impulsive flare phase the termination shock is expected to be formed, this could indicate the presence of this termination shock. However, this would be only indirect evidence of this kind of shock. Therefore, to gain further evidence, multifrequency studies are necessary. If the n-distribution is formed by the termination shock, it follows that the upstream plasma must be Maxwellian (or very close to it).

From an observational and diagnostic point of view, it is important to realize that in the space of reflected electrons there are also electrons of the seed distribution function. Therefore, for diagnostic purposes, the total distribution function needs to be considered. In the next paper, we plan to study effects of these electron distribution functions on intensities of the soft X-ray emission lines. This paper made the first necessary steps. It proved that reflected electrons at a shock had very similar distribution functions to n-distribution functions in their high-energy parts, which are used to interpret the observed soft X-ray emission lines.

Acknowledgements. M.V. was supported by projects 14-19376S and 15-17490S from the Grant Agency of the Czech Republic and by the European grant FP7-SHOCK 2284515. M.K. acknowledge support from Grants P209/12/0103 of the Grant Agency of the Czech Republic, the European grant FP7-SPACE-2013-1 F-CHROMA (No. 606862), and the Marie Curie FP7-PIRSES-GA-2011-295272 RadioSun project. This work is also supported by the CAS grant RVO:67985815.

References

Anderson, K., Lin, R., Martel, F., et al. 1979, Geophys. Res. Lett., 6, 401
Aulanier, G., Janvier, M., & Schmieder, B. 2012, A&A, 543, A110
Aurass, H., Vršnak, B., & Mann, G. 2002, A&A, 384, 273
Battaglia, M., Motorina, G., & Kontar, E. P. 2015, ApJ, 815, 73
Birn, J., & Priest, E. R. 2007, Reconnection of Magnetic Fields: Magnetohydrodynamics and Collisionless Theory and Observations (Cambridge: Cambridge Univ. Press)
Carmichael, H. 1964, NASA Spec. Publ., 50, 451
Chen, B., Bastian, T. S., Shen, C., et al. 2015, Science, 350, 1238
Decker, R. B. 1983, J. Geophys. Res., 88, 9959
Dryer, M., Andrews, M. D., Aurass, H., et al. 1998, Sol. Phys., 181, 159
Dzifčáková, E., & Karlický, M. 2008, Sol. Phys., 250, 329
Fahr, H. J., & Verscharen, D. 2016, A&A, 587, L1
Feldman, W., Anderson, R., Bame, S., et al. 1983, J. Geophys. Res., 88, 96
Goodrich, C. C., & Scudder, J. D. 1984, J. Geophys. Res., 89, 6654
Gopalswamy, N., Xie, H., Mäkelä, P., et al. 2013, Adv. Space Res., 51, 1981
Guo, F., & Giacalone, J. 2012, ApJ, 753, 28
Hares, J. D., Kilkenny, J. D., Key, M. H., & Lunney, J. G. 1979, Phys. Rev. Lett., 42, 1216
Hirayama, T. 1974, Sol. Phys., 34, 323
Karlický, M. 2012, ApJ, 750, 49
Karlický, M., Dzifčáková, E., & Dudík, J. 2012, A&A, 537, A36
Kopp, R. A., & Pneuman, G. W. 1976, Sol. Phys., 50, 85
Krauss-Varban, D., & Burgess, D. 1991, J. Geophys. Res., 96, 143
Krauss-Varban, D., & Wu, C. S. 1989, J. Geophys. Res., 94, 15367
Krimigis, S. M., Carbary, J. F., Keath, E. P., et al. 1981, J. Geophys. Res., 86, 8227
Kulinová, A., Kašparová, J., Dzifčáková, E., et al. 2011, A&A, 533, A81
Leroy, M. M., & Mangeney, A. 1984, Ann. Geophys., 2, 449
Livadiotis, G., & McComas, D. J. 2013, Space Sci. Rev., 175, 183
Morse, D. L. 1973, Plasma Phys., 15, 1262
Potter, D. W. 1981, J. Geophys. Res., 86, 11111
Seely, J. F., Feldman, U., & Doschek, G. A. 1987, ApJ, 319, 541
Sturrock, P. A. 1966, Nature, 211, 695
Sylwester, J., Gaicki, I., Kordylewski, Z., et al. 2005, Sol. Phys., 226, 45
Vaisberg, O. L., Zastenker, G. N., Klimov, S. I., Nozdrachev, M. N., & Borodkova, N. L. 1984, in Solar/Interplanetary Intervals, Proc. STIP Symp. held 4–6 August 1982, at St. Patrick's College, Maynooth, Ireland, eds. M. A. Shea, D. F. Smart, & S. M. P. McKenna-Lawlor, 407
Vandas, M. 1989a, Bull. Astr. Inst. Czechosl., 40, 175
Vandas, M. 1989b, Bull. Astr. Inst. Czechosl., 40, 189
Vandas, M. 1991, Bull. Astr. Inst. Czechosl., 42, 170
Vandas, M. 1994, ApJS, 90, 583
Vandas, M., & Karlický, M. 2000, Sol. Phys., 197, 85
Vandas, M., & Karlický, M. 2011, A&A, 531, A55
Vasyliunas, V. M. 1968, J. Geophys. Res., 73, 2839
Wu, C. S. 1984, J. Geophys. Res., 89, 8857